Eur. Phys. J. C (2024) 84:583
https://doi.org/10.1140/epjc/s10052-024-12933-0

THE EUROPEAN PHYSICAL JOURNAL C

Regular Article - Theoretical Physics

Schwarzschild black hole and redshift rapidity: a new approach towards measuring cosmic distances

Mehrab Momennia[1,2,a], **Pritam Banerjee**[3,b], **Alfredo Herrera-Aguilar**[1,c], **Ulises Nucamendi**[2,d]

[1] Instituto de Física, Benemérita Universidad Autónoma de Puebla, Apartado Postal J-48, 72570 Puebla, Puebla, Mexico
[2] Instituto de Física y Matemáticas, Universidad Michoacana de San Nicolás de Hidalgo, Edificio C-3, Ciudad Universitaria, CP 58040 Morelia, Michoacán, Mexico
[3] Indian Institute of Technology, Kharagpur 721302, India

Received: 24 March 2024 / Accepted: 20 May 2024

Abstract Motivated by recent achievements of a full general relativistic method in estimating the mass-to-distance ratio of supermassive black holes hosted at the core of active galactic nuclei, we introduce the new concept *redshift rapidity* in order to express the Schwarzschild black hole mass and its distance from the Earth just in terms of observational quantities. The redshift rapidity is also an observable relativistic invariant that represents the evolution of the frequency shift with respect to proper time in the Schwarzschild spacetime. We extract concise and elegant analytic formulas that allow us to disentangle mass and distance to black holes in the Schwarzschild background and estimate these parameters separately. This procedure is performed in a completely general relativistic way with the aim of improving the precision in measuring cosmic distances to astrophysical compact objects. Our exact formulas are valid on the midline and close to the line of sight, having direct astrophysical applications for megamaser systems, whereas the general relations can be employed in black hole parameter estimation studies. We also computed the frequency shift and the redshift rapidity for emitter eccentric orbits and calculated their relative error with respect to their numerical exact value for different eccentricities.

1 Introduction

Black holes first have been found just as mathematical solutions to Einstein field equations of the general relativity theory by Karl Schwarzschild whereas their existence in the cosmos has been recently approved through gravitational wave detections [1] and electromagnetic wave observations [2,3]. Moreover, investigating the motion of stars around the center of our galaxy has already provided convincing evidence for the presence of a supermassive black hole hosted at the core of the Milky Way galaxy [4–7].

Even though the aforementioned methods are fairly accurate in obtaining the black hole parameters using some types of observational data, they are not always applicable to other kinds of existing data from black holes and black hole environments. Therefore, we have been inventing and developing an independent general relativistic approach to measure the black hole and cosmological parameters [8–10]. This method is based on the observational frequency-shifted photons emitted by massive geodesic particles orbiting central black holes and has been initially suggested in [8], generalizing previous Keplerian models [11–13]. Recently, this approach has been developed to analytically express the mass and spin parameters of the Kerr black hole in terms of a few directly observational quantities [9]. Besides, it has been demonstrated that the Kerr black hole in asymptotically de Sitter background allows us to measure the Hubble constant and black hole parameters, simultaneously [10].

The initial method of [8] has been employed to obtain the kinematic redshift and blueshift in terms of black hole parameters for several black hole solutions, such as Kerr–Newman black holes in de Sitter spacetime [14], the Plebanski–Demianski black holes [15], higher dimensional Myers–Perry spacetime [16], and regular black holes in nonlinear electrodynamics [17]. Furthermore, a similar relation for the kinematic redshift has been found for black holes in modified gravity [18], black holes coupled to nonlinear electrodynam-

[a] e-mails: mmomennia@ifuap.buap.mx; momennia1988@gmail.com (corresponding author)
[b] e-mails: pritam@phy.iitkgp.ac.in; bpritamphy@gmail.com
[c] e-mail: aherrera@ifuap.buap.mx
[d] e-mails: ulises.nucamendi@umich.mx; unucamendi@gmail.com

Published online: 06 June 2024

ics [19], black holes immersed in a strong magnetic field [20], and the boson stars [21].

These studies have been performed based on the kinematic frequency shift which is not an observable quantity, unlike the total frequency shift of photons. Hence, this fact has motivated us to consider the total frequency shift as a directly observable element and extract concise and elegant analytic formulas for the mass and spin of the Kerr black hole in terms of few observable quantities [9]. With the help of this general relativistic method, the free parameters of polymerized black holes have been expressed in terms of the total redshift as well [22]. More recently, this approach has been extended to general spherically symmetric spacetimes in order to extract the information of free parameters of black holes in alternative gravitational theories beyond Einstein gravity [23].

From a practical point of view, the mass-to-distance ratio of several supermassive black holes hosted at the core of the active galactic nuclei (AGNs) NGC 4258 [24], TXS-2226-184 [25], and an additional 14 galaxies [26,27] has been estimated by employing this general relativistic approach. These supermassive black holes enjoy circularly orbiting water vapor clouds within accretion disks that emit redshifted photons toward a distant observer. This allows us to utilize the general relativistic method in order to estimate the Mass/Distance (M/D) ratio and quantify the gravitational redshift produced by the spacetime curvature which is a general relativistic effect.

In the parameter estimation studies of the supermassive black holes performed in [24–27], just the mass-to-distance ratio M/D of these compact objects has been estimated with the help of observational redshifted and blueshifted photons due to the fact that this ratio is degenerate in this general relativistic formalism. In this paper, we are going to introduce a new general relativistic invariant observable quantity, the *redshift rapidity*, which is the derivative of the redshift with respect to proper time. With the aid of the redshift rapidity, we shall disentangle M and D in the Schwarzschild background to extract concise and elegant analytic formulas for mass and distance to the black hole just in terms of observational elements. Thus, these formulas will help us to break the degeneracy in the M/D ratio of the Schwarzschild black hole and compute the mass and distance to the black hole separately. More recently, the redshift rapidity in the Reissner-Nordström black hole spacetime has been calculated and employed to extract analytic formulas for the black hole mass and charge as well as its distance from the Earth [28]. We would like to remark that these new formulas enable us to compute the distance to black holes and other astrophysical compact objects in a completely general relativistic framework with the aim of improving the precision in measuring cosmic distances with respect to previous post-Newtonian approaches that compute the angular-diameter distance to several megamaser galaxies like UGC 3789 [29], NGC 6264 [30], NGC 5765b [31], NGC 4258 [13,32], CGCG 074-064 [33], among others. We expect an improvement in precision because general relativity describes the gravitational phenomena in the compact objects' environment in a more complete way than the post-Newtonian approach.

The outline of this paper is as follows. The next section is devoted to a brief review of our general relativistic formalism in the Schwarzschild black hole spacetime. Then, we express the mass-to-distance ratio of the Schwarzschild black hole in terms of observable frequency shifts for three spacial points of the circular motion of orbiting massive particles, namely, on the midline and close to the line of sight (LOS). In Sect. 3, we define redshift rapidity as the proper time evolution of the frequency shift in the Schwarzschild background and employ this observable quantity in order to express the black hole mass and distance just in terms of observational elements on the midline and close to the LOS. We further present in Sects. 4 and 5, respectively, the frequency shift and the redshift rapidity for emitter eccentric orbits and calculate their relative error with respect to the numerical exact value of these quantities for different eccentricities in Sect. 6. We finish our paper with some concluding remarks in Sect. 7.

2 Schwarzschild black hole and the frequency shift

In order to describe our formalism to measure black hole parameters and cosmic distances, we start with a brief review on frequency shift formulas of massive probe particles in the Schwarzschild background based on [9]. The Schwarzschild black hole metric is given by the following line element

$$ds^2 = g_{tt}dt^2 + g_{rr}dr^2 + g_{\theta\theta}d\theta^2 + g_{\varphi\varphi}d\varphi^2, \tag{1}$$

with the metric components

$$g_{\mu\nu} = diag\left[-\left(1-\frac{2M}{r}\right), \left(1-\frac{2M}{r}\right)^{-1}, r^2, r^2\sin^2\theta\right], \tag{2}$$

where M is the total mass of the black hole and the event horizon is located at the Schwarzschild radius $r_+ = 2M$.

The massive geodesic particles revolving the Schwarzschild black hole feel the curvature of spacetime produced by the black hole mass and keep memory of it. Besides, the observers located on these particles can exchange redshifted photons that have information about the Schwarzschild black hole mass in their frequency shift from emission till detection. Thus, the shifts in the frequency of photons along with the orbital parameters of the emitter can be used to determine the black hole parameters [24–27]. Therefore, this formalism allows one to compute the black hole parameters in terms of directly measured observational quantities and the orbital parameters of the emitter [9,22,23].

Within General Relativity, the frequency of a photon that is emitted/detected by an emitter/observer with the proper 4-velocity $U_p^\mu = (U^t, U^r, U^\theta, U^\varphi)\,|_p$ at some position $x_p^\mu = (x^t, x^r, x^\theta, x^\varphi)\,|_p$ reads

$$\omega_p = -\left(k_\mu U^\mu\right)|_p, \tag{3}$$

where $k_p^\mu = \left(k^t, k^r, k^\theta, k^\varphi\right)|_p$ is the 4-momentum of the photons with the null condition $k_\mu k^\mu = 0$ and the index p refers to either the emission point x_e^μ or detection point x_d^μ of the photons. Additionally, the 4-velocity of particles is normalized to unity $U_\mu U^\mu = -1$, and when the detector's orbit is located far away from the emitter-black hole system, U_d^μ reduces to

$$U_d^\mu = (1, 0, 0, 0). \tag{4}$$

The frequency shift of light signals emitted by massive geodesic particles in equatorial circular orbits revolving the spherically symmetric background (1) is given by [8,9]

$$1 + z_{Schw} = \frac{\omega_e}{\omega_d} = \frac{(E_\gamma U^t - L_\gamma U^\varphi)\,|_e}{(E_\gamma U^t - L_\gamma U^\varphi)\,|_d}, \tag{5}$$

where the conserved quantities E_γ and L_γ stand for the total energy and axial angular momentum of the photons. By considering Eq. (4), this relation reduces to

$$1 + z_{Schw} = (U^t - b_\gamma U^\varphi)\,|_e, \tag{6}$$

for distant observers and $b_\gamma = L_\gamma/E_\gamma$ is the deflection of light parameter that takes into account the light bending generated by the gravitational field in the vicinity of the Schwarzschild black hole. The non-vanishing components of the 4-velocity of particles in the equatorial circular motion read [23]

$$U_e^t = \sqrt{\frac{2}{2g_{tt} - r g'_{tt}}}\bigg|_{r=r_e} = \sqrt{\frac{r_e}{r_e - 3M}}, \tag{7}$$

$$U_e^\varphi = \pm\frac{1}{r}\sqrt{\frac{r g'_{tt}}{2g_{tt} - r g'_{tt}}}\bigg|_{r=r_e} = \pm\frac{1}{r_e}\sqrt{\frac{M}{r_e - 3M}}, \tag{8}$$

where a prime denotes ∂_r, r_e is the radius of the emitter, and $+/-$ sign refers to counterclockwise/clockwise rotation of the emitter as seen by the observer.

In addition, the $(\varphi + \delta)$-dependent light bending parameter is given by [see Eq. (A.12) of the Appendix]

$$\begin{aligned} b_\gamma &= \frac{-g_{\varphi\varphi}\sin(\varphi+\delta)}{\sqrt{-g_{tt}}\sqrt{g_{\varphi\varphi}\sin^2(\varphi+\delta) + r_e^2 g_{rr}\cos^2(\varphi+\delta)}} \\ &= -\frac{r_e^{3/2}\sin(\varphi+\delta)}{\sqrt{r_e - 2M\sin^2(\varphi+\delta)}}, \end{aligned} \tag{9}$$

where φ is the unobservable azimuthal angle ranging $0 \leq \varphi \leq 2\pi$ and δ is the aperture angle of the telescope (angular distance) that is a measurable quantity (see Fig. 5 of the Appendix). Both φ and δ are positive (negative) when measured counterclockwise (clockwise) with respect to the LOS.

Now, by substituting Eqs. (7)–(9) into the redshift formula (6), we can find the frequency shift of photons emitted by massive geodesic particles on an arbitrary point of equatorial circular orbits in the Schwarzschild background as follows

$$\begin{aligned} 1 + z_{Schw} &= \sqrt{\frac{r_e}{r_e - 3M}} \\ &\times\left(1 \pm \sqrt{\frac{M}{r_e - 2M\sin^2(\varphi+\delta)}}\sin(\varphi+\delta)\right), \end{aligned} \tag{10}$$

with the contribution of the gravitational redshift z_g and the kinematic redshift $z_{kin_\pm}$ as

$$z_g = -1 + \sqrt{\frac{r_e}{r_e - 3M}}, \tag{11}$$

$$z_{kin_\pm} = \pm\sqrt{\frac{r_e}{r_e - 3M}}\sqrt{\frac{M}{r_e - 2M\sin^2(\varphi+\delta)}}\sin(\varphi+\delta), \tag{12}$$

satisfying $z_{Schw} = z_g + z_{kin_\pm}$. In what follows we shall restrict ourselves to the counterclockwise motion of the emitter as seen by a distant observer, using the + sign in Eqs. (8), (10), and (12) in order to avoid any ambiguity.

In the Newtonian limit $M/r_e \to 0$, the frequency shift in the Schwarzschild spacetime (10) reduces to the projection of the Keplerian velocity of a particle in circular motion on the LOS in the following way

$$z_N = \sqrt{\frac{M}{r_e}}\sin(\varphi+\delta) + \mathcal{O}\left(\frac{M}{r_e}\right), \tag{13}$$

as we expected. Besides, in this case the azimuthal angle φ is a function of the observable δ for an arbitrary point on the circular orbit as follows [see Eq. (A.17) of the Appendix]

$$\delta = \arccos\left(\frac{D - r_e\cos\varphi}{\sqrt{D^2 + r_e^2 - 2Dr_e\cos\varphi}}\right), \tag{14}$$

where D is the radial distance between the black hole center and the observer.

Figure 1 illustrates the redshift formula (10) versus the azimuthal angle φ. This figure shows how the frequency shift in the Schwarzschild spacetime changes with the motion of the massive test particle and the non-vanishing value of the frequency shift at the LOS indicates the gravitational redshift. Besides, on the midline where $\varphi \approx \pm\pi/2$, the total frequency shift is maximal, hence easier to be identified observationally. The range of azimuthal angle used to plot Fig. 1 is determined to respect the assumption underlying Eq. (14), which considers that light bending is minimal.

In order to express the mass-to-distance ratio of the Schwarzschild black hole in terms of observational quanti-

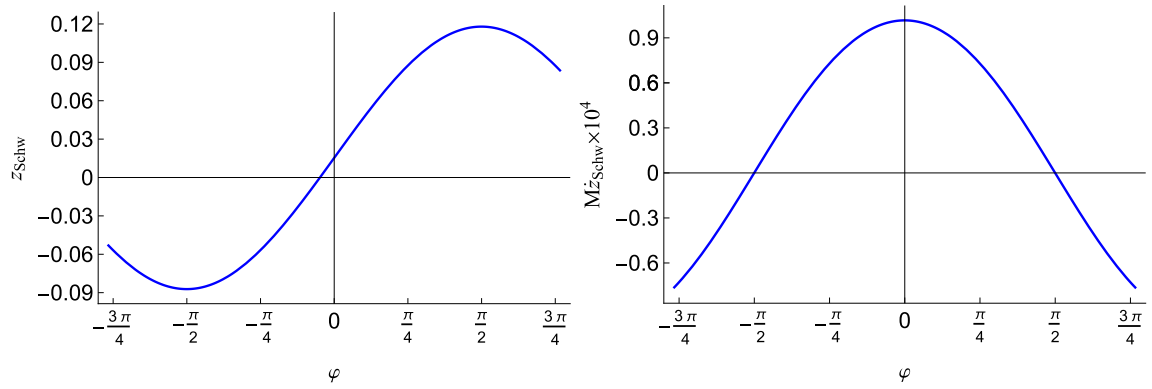

Fig. 1 The frequency shift z_{Schw} (left panel) and the redshift rapidity $\dot{z}_{Schw}$ (right panel) versus the azimuthal angle in the Schwarzschild background for $r_e = 10^2 M$ and $D = 10^5 M$. The shift in the frequency is maximal close to the midline where $\varphi \approx \pm\pi/2$, whereas the maximum redshift rapidity is at the LOS $\varphi = 0$. In Eqs. (10) and (23), we replaced δ with Eq. (14) to plot these curves

ties, it is convenient to consider two special important cases useful for describing the frequency shift of photon sources within accretion disks revolving supermassive black holes hosted at the core of AGNs.

2.1 Midline case

The first case is related to highly shifted frequency photons emitted from particles located at the midline where $\varphi = \pm\pi/2$. The position vector of these particles with respect to the black hole center is orthogonal to the observer's LOS. Hence, by substituting $\varphi = \pm\pi/2$ in the frequency shift formula (10), one can find the highly redshifted ($\varphi = +\pi/2$) and blueshifted ($\varphi = -\pi/2$) photons as below

$$1 + z^m_{Schw_{1,2}} = \sqrt{\frac{r_e}{r_e - 3M}}\left(1 \pm \sqrt{\frac{M}{r_e - 2M\cos^2\delta_m}}\cos\delta_m\right) \tag{15}$$

where the index "m" means the aperture angle δ should be measured on the midline and now the plus (minus) sign refers to the redshifted (blueshifted) photons denoted by $z^m_{Schw_1}$ ($z^m_{Schw_2}$) on the midline. By multiplying $R_m := 1 + z^m_{Schw_1}$ and $B_m := 1 + z^m_{Schw_2}$, it is straightforward to obtain the mass-to-distance ratio of the Schwarzschild black hole in terms of observational quantities on the midline as follows

$$\frac{M}{D\delta_m} = \frac{R_m B_m - 1}{2R_m B_m} - \frac{(1 - R_m B_m)(3 - 4R_m B_m)}{6R_m B_m (3 - R_m B_m)}\delta^2_m, \tag{16}$$

where we used the approximation (A.15) where $D \gg r_e$ is the radial distance between the black hole and the detector. Additionally, we considered the limit $\delta_m \to 0$ in consistency with the condition (4) for distant observers as well. As we can see from Eq. (16), the mass-to-distance ratio of the Schwarzschild black hole is expressed in terms of directly observational elements $\{R_m, B_m, \delta_m\}$.

2.2 Line of sight case

The second case is describing the frequency shift of photons emitted close to the LOS where $\varphi \to 0$. Hence, by substituting $\varphi = \varphi_s \sim 0$ in the frequency shift formula (10), we find the expressions for slightly redshifted and slightly blueshifted photons as below

$$1 + z^s_{Schw_{1,2}} = \sqrt{\frac{r_e}{r_e - 3M}} \pm \sqrt{\frac{M}{r_e - 3M}}\,(\varphi_s + \delta_s)\,, \tag{17}$$

where the index "s" means the measurement should be performed for systemic particles (particles close to the LOS) and we applied the limit $\delta_s \to 0$ simultaneously. Additionally, we have just the gravitational redshift z_g exactly at the LOS with $\varphi_s = 0 = \delta_s$. In this relation, the angles δ_s and φ_s should be measured close to the LOS, and the plus (minus) sign refers to the redshifted (blueshifted) photons close to the LOS denoted by $z^s_{Schw_1}$ ($z^s_{Schw_2}$), respectively. Now, by multiplying $R_s := 1 + z^s_{Schw_1}$ and $B_s := 1 + z^s_{Schw_2}$, we can obtain the mass-to-distance ratio of the Schwarzschild black hole close to the LOS as follows

$$\frac{M\varphi_s}{D\delta_s} = \frac{R_s B_s - 1}{3R_s B_s} + \mathcal{O}\left(\varphi^2_s\right), \tag{18}$$

in which we used the approximation $r_e \sim D\delta_s/\varphi_s$ from Eq. (A.16) valid close to the LOS and considered the limits $\{\delta_s \to 0, \varphi_s \to 0\}$ simultaneously to derive this equation. Furthermore, this relation is a function of a set of purely observational quantities $\{R_s, B_s\}$.

If we combine the result (18), valid for close to the LOS azimuthal angles, with the midline relation (16), we can express φ_s in terms of purely observational quantities $\{R_m, B_m, \delta_m; R_s, B_s, \delta_s\}$.

3 Disentangling mass and distance: the role of redshift rapidity

The mass-to-distance ratio formulas (16) and (18) of the Schwarzschild black hole can be employed to estimate the M/D ratio of real astrophysical systems as it was accomplished for the central supermassive black holes of 17 galaxies in [24–27]. As the next step in this direction, we are going to disentangle the mass M and the distance to the black hole D to obtain closed formulas for each parameter in terms of the set of observational elements $\{R_m, B_m, \delta_m; R_s, B_s, \delta_s\}$. In order to achieve this aim, we define the frequency shift rapidity, henceforth called *redshift rapidity*, as the proper time evolution of the frequency shift z_{Schw} (6) in the Schwarzschild background as follows

$$\dot{z}_{Schw,e} = \frac{dz_{Schw}}{d\tau} = \frac{d}{d\tau}(U_e^t - b_\gamma U_e^\varphi), \tag{19}$$

which is the redshift rapidity at the emission point and constitutes a general relativistic invariant quantity since the proper time also shares this property. Notwithstanding, we should note that the redshift rapidity needs to be measured from the Earth. Therefore, by making use of the chain rule, we rewrite Eq. (19) at the observer position as

$$\dot{z}_{Schw} = \frac{dz_{Schw}}{dt} = \frac{d\tau}{dt}\frac{dz_{Schw}}{d\tau} = \frac{1}{U_e^t}\frac{d}{d\tau}(U_e^t - b_\gamma U_e^\varphi), \tag{20}$$

which is an observable quantity that we measure here on the Earth. For massive geodesic particles circularly orbiting the black hole in the equatorial plane, the redshift rapidity (20) reduces to

$$\dot{z}_{Schw} = -\frac{db_\gamma}{d\tau}\frac{U_e^\varphi}{U_e^t}, \tag{21}$$

since the t-component U_e^t (7) and φ-component U_e^φ (8) of the 4-velocity are constant quantities for circular orbits whereas the light bending parameter (9) is time dependent through δ and φ. By employing the chain rule, we have

$$\dot{z}_{Schw} = -\left(\frac{\partial b_\gamma}{\partial \varphi} + \frac{\partial b_\gamma}{\partial \delta}\frac{\partial \delta}{\partial \varphi}\right)\frac{(U_e^\varphi)^2}{U_e^t}, \tag{22}$$

where we used $U_e^\varphi = \frac{d\varphi}{d\tau}\Big|_{r=r_e}$. Now, we perform the aforementioned derivatives by taking into account the light bending parameter (9) and the $\delta(\varphi)$-relation (14) to obtain the redshift rapidity for an arbitrary point on the circular orbit as below

$$\dot{z}_{Schw} = \frac{1}{\left[r_e - 2M\sin^2(\varphi+\delta)\right]^{\frac{3}{2}}} \times \frac{DM\,(D - r_e\cos\varphi)\cos(\varphi + \delta)}{\sqrt{r_e - 3M}\left(D^2 + r_e^2 - 2Dr_e\cos\varphi\right)}. \tag{23}$$

Figure 1 shows the behavior of the redshift rapidity versus the azimuthal angle φ. As one can see from this figure, the redshift rapidity at the LOS is maximal, hence it is easier to measure this quantity at $\varphi \approx 0$.

It is worth noting that the redshift rapidity (23) reduces to the projection of the Keplerian acceleration of a particle in circular motion on the LOS in the Newtonian limit $M/r_e \to 0$ and large distances $r_e/D \to 0$

$$\dot{z}_N = \frac{M}{r_e^2}\cos(\varphi+\delta) + \mathcal{O}\left(\frac{M^2}{r_e^3}\right), \tag{24}$$

as it should be.

As the final step, based on the emitter-black hole system configuration and observational data availability, we can employ the redshift rapidity (23) as well as either Eq. (16) or Eq. (18) to disentangle the Schwarzschild black hole mass M and the distance to the black hole D. Here, we are going to disentangle M and D for two important cases describing astrophysical photon sources within accretion disks circularly orbiting central supermassive black holes at the core of AGNs.

3.1 Midline case

The first important case is related to the emitters on the midline where their emitted photons are highly redshifted/blueshifted. The mass-to-distance ratio of the central black hole in terms of these frequency shifted photons is given in Eq. (16). In order to find the redshift rapidity of the same redshifted particles, we substitute the approximation (A.15) for r_e in the redshift rapidity relation (23) and consider the limit $\delta_m \to 0$ to get

$$\dot{z}^m_{Schw} = \frac{\frac{M}{D\delta_m}}{D\sqrt{1-3\frac{M}{D\delta_m}}\left(1-2\frac{M}{D\delta_m}\right)^{\frac{3}{2}}} \times \left(1 + \frac{11 - 28\frac{M}{D\delta_m} - 12\left(\frac{M}{D\delta_m}\right)^2}{6\left(1-3\frac{M}{D\delta_m}\right)\left(1-2\frac{M}{D\delta_m}\right)}\delta_m^2\right), \tag{25}$$

up to second order in δ_m. Finally, one can find the explicit form of the Schwarzschild black hole mass and distance to the black hole by solving Eqs. (16) and (25) as below

$$M = \frac{(R_m B_m - 1)^2}{2\dot{z}^m_{Schw}\sqrt{6 - 2R_m B_m}}\delta_m + \mathcal{O}\left(\delta_m^3\right), \tag{26}$$

$$D = \frac{R_m B_m\,(R_m B_m - 1)}{\dot{z}^m_{Schw}\sqrt{6 - 2R_m B_m}} \times \left(1 + \frac{R_m B_m(3R_m B_m - 7)(8R_m B_m - 27) - 36}{6(R_m B_m - 3)^2}\delta_m^2\right), \tag{27}$$

fully expressed in terms of observational quantities $\{R_m, B_m, \dot{z}^m_{Schw}, \delta_m\}$ that should be measured on the midline.

3.2 Line of sight case

The second important case belongs to the photon sources that lie close to the LOS where their emitted photons are slightly redshifted/blueshifted but have maximum redshift rapidity. The mass-to-distance ratio of the central black hole in terms of these frequency shifted photons is given by Eq. (18). Thus, we substitute $r_e = D\delta_s/\varphi_s$ from the approximation (A.16) into the redshift rapidity formula (23) and apply the limits $\{\delta_s \to 0, \varphi_s \to 0\}$ to get

$$\dot{z}^s_{Schw} = \frac{1}{M}\left(1 - 3\frac{M\varphi_s}{D\delta_s}\right)^{-\frac{1}{2}}\left(\frac{M\varphi_s}{D\delta_s}\right)^2, \tag{28}$$

for the photon sources close to the LOS. Now, by substituting Eq. (18) in this relation, we can find the Schwarzschild black hole mass as follows

$$M = \frac{(R_s B_s - 1)^2}{9\dot{z}^s_{Schw}\,(R_s B_s)^{\frac{3}{2}}}, \tag{29}$$

fully in terms of observational quantities $\{R_s, B_s, \dot{z}^s_{Schw}\}$ that should be measured close to the LOS. As the next step, we take advantage of this relation and Eq. (16) in order to combine observations from both midline and LOS to get the distance to the black hole as

$$D = \frac{(R_s B_s - 1)^2}{9\dot{z}^s_{Schw}\,(R_s B_s)^{\frac{3}{2}}}\frac{2R_m B_m}{\delta_m\,(R_m B_m - 1)}, \tag{30}$$

which is a significant relation because it contains information on both high-frequency shifted particles on the midline $\{R_m, B_m\}$ and maximum redshift rapidity close to the LOS $\dot{z}^s_{Schw}$ (see Fig. 1 and related discussion). From an observational point of view, this formula is important due to the fact that it is easier to identify frequency shifts on the midline and the redshift rapidity close to the LOS.

4 Frequency shift in case of elliptical orbit of the emitter

So far, we have discussed the redshift and redshift rapidity, considering that the emitter is in a circular orbit. While circularity is a very good assumption, the emitter orbit may differ from the circularity and acquire a small eccentricity in real astrophysical situations. Keeping this in mind, we, in this section, undertake the above analysis using an elliptical emitter orbit. Next, we set the eccentricity to be small and express the relations up to the first order in eccentricity.

In the Schwarzschild metric, we can consider the emitter to be orbiting in the equatorial plane with 4-velocity $U^\mu_e = \{U^t_e, U^r_e, 0, U^\varphi_e\}$ without loss of generality. From the 4-velocity normalization of timelike particles in the Schwarzschild background, we can write

$$(U^r_e)^2 = E^2 - (r_e - 2M)\left(\frac{1}{r_e} + \frac{L_z^2}{r_e^3}\right), \tag{31}$$

where E and L_z are constants of motion, namely, the orbital energy and z-component of the orbital angular momentum of the emitter particle, respectively, defined as,

$$E = \left(1 - \frac{2M}{r_e}\right)U^t, \quad L_z = r_e^2 U^\varphi. \tag{32}$$

We can rewrite Eq. (31) as

$$(U^r_e)^2 = 2\epsilon - 2v(r_e), \tag{33}$$

where

$$2\epsilon = E^2 - 1, \quad 2v(r_e) = \frac{L_z^2}{r_e^2}\left(1 - \frac{2M}{r_e}\right) - \frac{M}{r_e}. \tag{34}$$

Throughout the elliptical orbit, E and L_z remain fixed. We express the orbital radius of the emitter as

$$r_e = \frac{p}{1 + e\cos\chi}, \tag{35}$$

where p is the semi-latus rectum, e is the eccentricity of the elliptical orbit, and χ is the angular position of the emitter measured from the semi-major axis such that $\chi = 0$ stands for the pericenter position. Using the fact that at the pericenter $r_e = r_p$ and apocenter $r_e = r_a$ of the elliptical orbit, $U^r_e(r_p) = 0 = U^r_e(r_a)$, we can use Eq. (33) to find E and L_z as

$$E = \sqrt{\frac{p^2 - 4pM + 4M^2(1 - e^2)}{p\left(p - M(e^2 + 3)\right)}}, \tag{36}$$

$$L_z = \pm\sqrt{\frac{Mp^2}{p - M(e^2 + 3)}}. \tag{37}$$

Here, according to our convention, the plus (minus) sign in Eq. (37) stands for the counterclockwise (clockwise) rotation of the emitter as seen by the observer. Now, putting Eqs. (36) and (37) in (33)–(34) we get

$$U^r_e = \pm\, e\sin\chi\left[\frac{pM - 2M^2\,(3 + e\cos\chi)}{p^2 - pM(e^2 + 3)}\right]^{1/2}. \tag{38}$$

Note that U^r_e can take the plus (minus) sign for the emitter's counterclockwise (clockwise) motion. From Eqs. (32), (36), and (37), we can further obtain the other two components of the 4-velocity. The sign of U^φ_e is the same as that of L_z. It follows our convention that φ and δ are again positive (negative) when measured counterclockwise (clockwise) from the LOS.

Now, let us discuss the relation between χ and φ. After taking derivative of Eq. (35) with respect to proper time of the emitter and doing some algebra using Eqs. (32), (37), and (38) we get

$$\frac{d\varphi}{d\chi} = \left[1 - (3 + e\cos\chi)\frac{2M}{p}\right]^{-1/2}. \tag{39}$$

The above equation holds information about the general relativistic precession of the emitter's elliptical orbit around the black hole. To simplify our convention, we choose that χ and the azimuthal angle φ increase in the same direction. We need to solve Eq. (39) for χ to replace it in terms of φ in our formalism. However, in the case of large p, we can get a simple linear relation, i.e., $\chi = \varphi + \varphi_0$. The constant phase φ_0 is related to the orientation of the elliptical orbit with respect to the LOS (see Fig. 2).

In fact, the precession of the angle at which the radial coordinate attains its maximum/minimum value (apocenter/pericenter) is a property of the geodesic motion of the photon sources. The measurement of this quantity requires the observation of several orbital cycles of the emitter and hence, does not influence our calculations of M and D, which is based on measurements at specific points of the orbit of the emitter.

Furthermore, the light bending parameter is found similarly as before

$$b_\gamma = -\frac{r_e^{3/2}\sin(\varphi+\delta)}{\left[r_e - 2M\sin^2(\varphi+\delta)\right]^{1/2}}. \tag{40}$$

Following the convention adopted in (9), b_γ is negative (positive) on the right (left) hand side of LOS. Therefore, for counterclockwise motion, b_γ must have a minus sign on the right of LOS to yield a redshifted photon and vice versa for clockwise motion.

Now, we can use the definition of frequency shift in Eq. (5) for elliptical orbits and obtain

$$1 + z_{Schw} = \frac{\omega_e}{\omega_d} = \frac{\left(E_\gamma U^t - g_{rr}k^r U^r - L_\gamma U^\varphi\right)|_e}{\left(E_\gamma U^t - g_{rr}k^r U^r - L_\gamma U^\varphi\right)|_d}, \tag{41}$$

and as before, we consider the detector to be located far away from the emitter, thus obtaining

$$1 + z_{Schw} = \left(U^t - g_{rr}\frac{k^r}{E_\gamma}U^r - b_\gamma U^\varphi\right)\Big|_e. \tag{42}$$

Using Eqs. (A.5) and (40), we get

$$\frac{k^r_e}{E_\gamma} = \frac{\cos(\varphi+\delta)}{\left[1 - \frac{2M}{r_e}\sin^2(\varphi+\delta)\right]^{1/2}}. \tag{43}$$

Here, $E_\gamma > 0$, and k^r is positive if $-\pi/2 < (\varphi+\delta) < \pi/2$ (emitter is located at the front), and negative if $(\varphi+\delta) < -\pi/2$ and $\varphi+\delta > \pi/2$ (emitter is located at the back). Thus, the sign of k^r/E_γ is automatically defined by $(\varphi+\delta)$.

Now, replacing Eqs. (32), (38), (40), and (43) in Eq. (42), we can obtain an exact formula for the frequency shift including arbitrary values of the eccentricity e as below

$$1 + z_{Schw} = \frac{1}{\sqrt{c_1}f r_e}\left(\sqrt{c_1}c_3 r_e + \frac{c_2 f M r_e \sin(\delta+\varphi)}{c_4^2 r_e} - c_2 e r_e\sqrt{f - 4c_4^2}\sin\chi\cos(\delta+\varphi)\right), \tag{44}$$

where the parameters f and c_i $(i = 1, 2, 3, 4)$ are given by

$$f = 1 - \frac{2M}{r_e}, \quad c_1 = 1 - \frac{2M\sin^2(\delta+\varphi)}{r_e}, \tag{45}$$

$$c_2 = \sqrt{\frac{M}{r_e(1+e\cos\chi) - \left(e^2+3\right)M}}, \tag{46}$$

$$c_3 = \frac{c_2}{c_4}\sqrt{4c_4^4\left(1-e^2\right) - 4c_4^2 + 1}, \tag{47}$$

$$c_4 = \sqrt{\frac{M}{r_+(1+e\cos\chi)}}. \tag{48}$$

Now, in what follows we consider a first-order approximation in e. Thus, in the far-away observer limit $D \gg r_e$, we get

$$\begin{aligned} 1 + z_{Schw} = \sqrt{\frac{r_e}{r_e - 3M}}\Bigg[1 &\pm \mathcal{A}\sin(\varphi+\delta) \\ &+ \Bigg(\frac{M(r_e-6M)}{2(r_e-3M)(r_e-2M)}\cos\chi \\ &\pm \frac{\mathcal{A}(r_e-6M)}{2(r_e-3M)}\cos\chi\sin(\varphi+\delta) \\ &\mp \frac{\mathcal{A}\sqrt{r_e(r_e-6M)}}{r_e-2M}\cos(\varphi+\delta)\sin\chi\Bigg)e\Bigg] + \mathcal{O}(e^2), \end{aligned} \tag{49}$$

where $\chi \approx \varphi + \varphi_0$ and

$$\mathcal{A} = \sqrt{\frac{M}{r_e - 2M\sin^2(\varphi+\delta)}}. \tag{50}$$

In the above Eq. (49), the upper (lower) sign stands for the counterclockwise (clockwise) motion of the emitter. Note that a redshifted photon is generated in two ways: on the right-hand side of the LOS for a counterclockwise motion and on the left of LOS for a clockwise motion. Both ways are physically equivalent which can be confirmed from Eq. (49).

In the Newtonian limit, i.e., $D \gg r_e \gg M$, we can further simplify Eq. (49) as

$$z_N = \pm\sqrt{\frac{M}{r_e}}\sin(\varphi+\delta)$$

$$\times\left[1+\left(\frac{1}{2}\cos\chi-\sin\chi\cot(\varphi+\delta)\right)e\right]+\mathcal{O}\left(\frac{M}{r_e}\right). \tag{51}$$

5 Redshift rapidity in case of elliptical orbit of the emitter

Here, we calculate the redshift rapidity in the case of an eccentric emitter orbit. Next, we shall present formulas for small eccentricity as well. We define redshift rapidity as

$$\frac{dz}{dt}=\frac{dz}{d\tau}\frac{d\tau}{dt}=\frac{1}{U_e^t}\Bigg[\frac{dU_e^t}{d\tau}-b_\gamma\frac{dU_e^\phi}{d\tau}-\frac{db_\gamma}{d\tau}U_e^\phi - g_{rr}\frac{dU_e^r}{d\tau}\frac{k_e^r}{E_\gamma}-\frac{dg_{rr}}{d\tau}U_e^r\frac{k_e^r}{E_\gamma}-g_{rr}U_e^r\frac{d}{d\tau}\left(\frac{k_e^r}{E_\gamma}\right)\Bigg]. \tag{52}$$

By using Eqs. (31)–(32), we get

$$\frac{dU_e^r}{d\tau}=\frac{1}{r_e}\left[\frac{L_z^2}{r_e^2}\left(1-\frac{3M}{r_e}\right)-\frac{M}{r_e}\right], \tag{53}$$

$$\frac{dU_e^\phi}{d\tau}=-\frac{2L_z}{r_e^3}U_e^r, \tag{54}$$

$$\frac{dU_e^t}{d\tau}=-\frac{2ME}{(r_e-2M)^2}U_e^r. \tag{55}$$

Again, from the null condition $k_\mu k^\mu=0$, we can obtain the derivative of k_e^r/E_γ as follows

$$\frac{d}{d\tau}\left(\frac{k_e^r}{E_\gamma}\right)=\frac{(r_e-3M)b_\gamma^2U_e^r-r_e(r_e-2M)b_\gamma\frac{db_\gamma}{d\tau}}{r_e^{5/2}\sqrt{b_\gamma^2(2M-r_e)+r_e^3}}. \tag{56}$$

On the other hand, by employing the chain rule, we have

$$\frac{db_\gamma}{d\tau}=\left(\frac{\partial b_\gamma}{\partial r}U_e^r+\frac{\partial b_\gamma}{\partial\varphi}U_e^\varphi+\frac{\partial b_\gamma}{\partial\delta}\frac{\partial\delta}{\partial\varphi}U_e^\varphi\right), \tag{57}$$

where $\frac{\partial\delta}{\partial\varphi}$ is obtained from Eq. (A.17). By calculating the terms presented in Eq. (52), we can find the redshift rapidity for arbitrary eccentric orbits as follows

$$\frac{dz_{Schw}}{dt}=-\frac{f}{c_3r_e^2}\Bigg[\frac{c_2c_8M}{c_4^2}+\frac{2c_3c_4c_5eM\sin\chi}{f^2}-\frac{M\cos(\delta+\varphi)}{\sqrt{c_1}f}\times\left(1+\frac{c_2^2M(3M-r_e)}{c_4^2r_e^2}\right)-\frac{2c_4^2c_5^2e^2M\sin^2\chi\cos(\delta+\varphi)}{\sqrt{c_1}f^2}+\frac{2c_4c_5e\sin\chi\sin(\delta+\varphi)}{\sqrt{c_1}}\left(\frac{c_2M}{c_4^2}+\frac{\sqrt{c_1}c_8r_e}{2\sqrt{c_1-f\sin^2(\delta+\varphi)}}-\frac{c_4c_5e(3M-r_e)\sin\chi\sin(\delta+\varphi)}{2f\sqrt{c_1-f\sin^2(\delta+\varphi)}}\right)\Bigg], \tag{58}$$

where the parameters c_i $(i=5,6,7,8)$ are given by

$$c_5=\sqrt{\frac{r_e(1+e\cos\chi)-2M(3+e\cos\chi)}{r_e(1+e\cos\chi)-\left(e^2+3\right)M}}, \tag{59}$$

$$c_6=-\frac{\cos(\delta+\varphi)}{\sqrt{c_1}}\left(\frac{2M\sin^2(\delta+\varphi)}{c_1}+r_e\right), \tag{60}$$

$$c_7=\frac{\sin(\delta+\varphi)}{\sqrt{c_1}}\left(\frac{M\sin^2(\delta+\varphi)}{c_1r_e}-1\right), \tag{61}$$

$$c_8=\frac{c_2c_6(1+e\cos\chi)(D\cos\varphi-r_e)}{D^2+r_e^2-2r_eD\cos\varphi}+\frac{c_2c_6M}{c_4^2r_e^2}+c_4c_5c_7e\sin\chi. \tag{62}$$

This redshift rapidity formula (58) takes the following form in the limit of a faraway observer, $D\gg r_e$, as

$$\frac{dz}{dt}=\frac{\mathcal{A}^3M^{-1/2}}{\sqrt{r_e-3M}}\cos(\varphi+\delta)+\sqrt{\frac{r_e-6M}{r_e-3M}}\times\Bigg[\mp\frac{2M^{3/2}}{r_e^{3/2}(r_e-2M)}\sin\chi+\mathcal{A}^3M^{1/2}\Bigg(\frac{\sqrt{r_e-6M}}{2(r_e-2M)(r_e-3M)}\cos(\varphi+\delta)\cos\chi+\frac{2\sqrt{r_e-6M}}{r_e(r_e-2M)}\sin^2(\varphi+\delta)\cos(\varphi+\delta)\cos\chi+\frac{1}{r_e^{3/2}}\sin^3(\varphi+\delta)\sin\chi\Bigg)\Bigg]e+\mathcal{O}(e^2), \tag{63}$$

where $\mathcal{A}$ is defined in Eq. (50). For the counterclockwise motion of the emitter, redshift rapidity is plotted for various orientations of elliptical orbits (see top right panel of Fig. 2). Similar to the frequency shift, we see from Eq. (63) that redshift rapidity on the right-hand side of LOS for counterclockwise motion (upper sign) is equivalent to that on the left-hand side of LOS for clockwise motion (lower sign).

In the Newtonian limit $D\gg r_e\gg M$, Eq. (63) is simplified further as follows

$$\frac{dz_N}{dt}=\frac{M}{r_e^2}\cos(\varphi+\delta)\mp e\frac{2M^{3/2}}{r_e^{5/2}}\sin\chi+\mathcal{O}\left(\frac{M^2}{r_e^3}e\right). \tag{64}$$

It is worth mentioning that there exist measurements of the redshift rapidity for some megamaser systems in the accretion disks of supermassive black holes hosted at the center of AGNs, such as UGC 3789 [29], NGC 6264 [30], NGC 5765b [31], CGCG 074-064 [33] that are reported as "accelerations" of the photon sources. These measured redshift

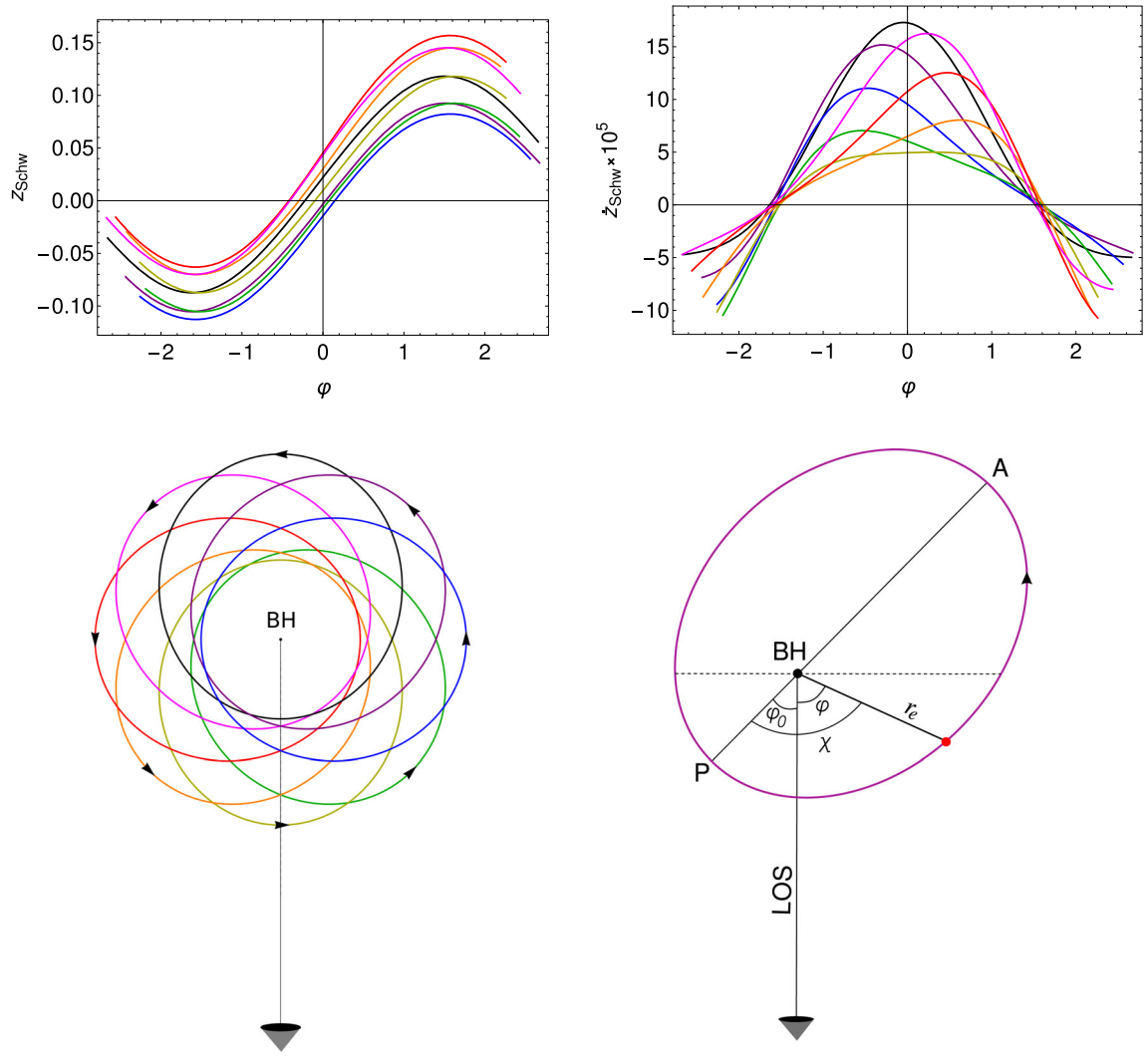

Fig. 2 Top left panel: The frequency shift z_{Schw} versus the azimuthal angle in the Schwarzschild background for $M = 1$, $p = 100$, $e = 0.3$, and $D = 10^5$ considering the counterclockwise motion of the emitter. Different colors stand for various orientations of the orbits, i.e., $\varphi_0 = 0$ to 2π in intervals of $\pi/4$ (see bottom left panel). The deviation in the frequency shift due to orbital orientations is maximal close to the midline where $\varphi \approx \pm\pi/2$. Top right panel: Redshift rapidity versus the azimuthal angle for the same system. Bottom left panel: A schematic diagram showing the orientations of the elliptical orbits used to plot the top panels. Each color indicates an orbit with a fixed φ_0. The arrow denotes the counterclockwise motion of the emitter. Bottom right panel: The position of an emitter (red dot) is shown in an elliptical orbit along with the corresponding angular position φ measured from the LOS, χ measured from the semi-major axis (AP), and $\varphi_0 = \chi - \phi$. A and P denote the apocenter and pericenter positions, respectively. The midline is shown by the horizontal dashed line

rapidities range $[-1.68, 3.48]$ km/s/year for test particles emitting at the midline and lie within $[0.9, 8.4]$ km/s/year for photon sources located by the observer's line of sight. However, the corresponding errors lie in the ranges $[0.50, 3.36]$ and $[0.20, 3.07]$ km/s/year, which are quite big compared to the measured quantities.

Finally, one should note that, unlike the circular case, we cannot obtain analytic formulas for M and D in terms of observational quantities due to the complexity of the expressions (44) and (58). In this case, Eqs. (42) and (56) can be inverted numerically or one needs to rely on a Bayesian statistical fit of observational data and use Eqs. (44) and (58) simultaneously to determine M and D for non-circular orbits.

6 Error estimation of the frequency shift and the redshift rapidity formula

In Eqs. (49) and (63), we have expanded the frequency shift and the redshift rapidity up to the first order in eccentricity. Naturally, it is necessary to discuss the error included while ignoring the higher-order terms. To quantify that, we define

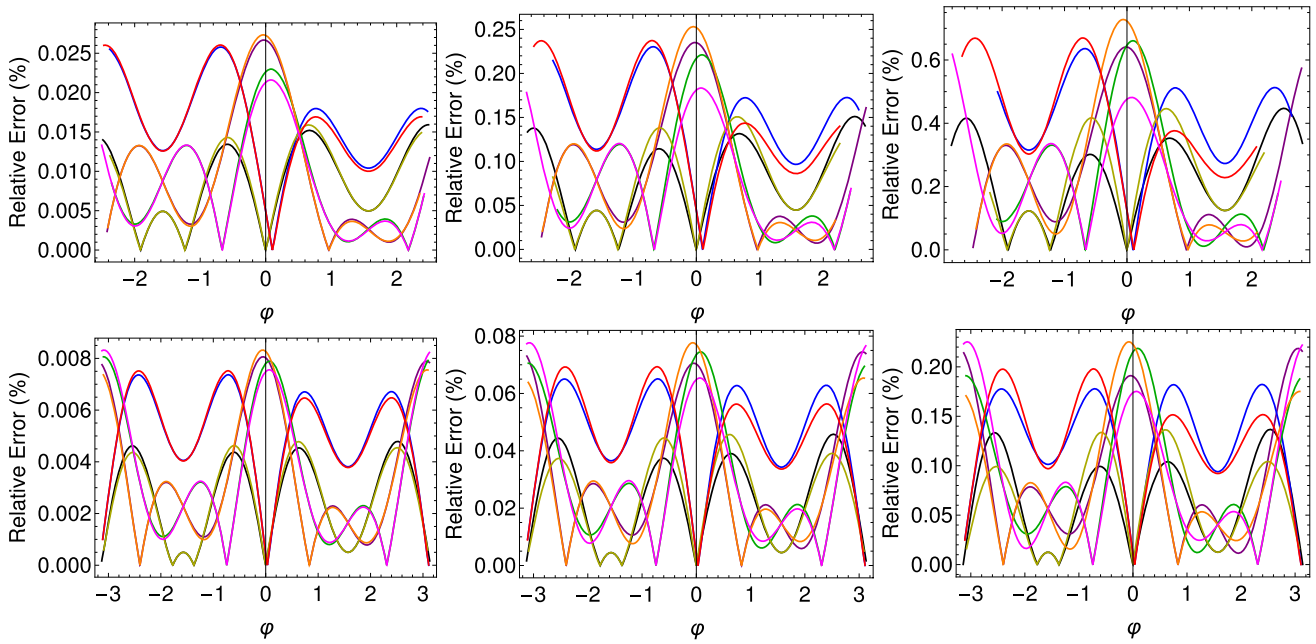

Fig. 3 Relative percentage error of frequency shift given by Eq. (65) for various values of orbital parameters p and e. The upper (lower) panels refer to $p = 100$ ($p = 1000$). Columns from left to right indicate $e = 0.1, 0.3, 0.5$, respectively. We have set $M = 1$, and a large value of $D = 1000p$. For various colors in each plot, see the bottom panel of Fig. 2

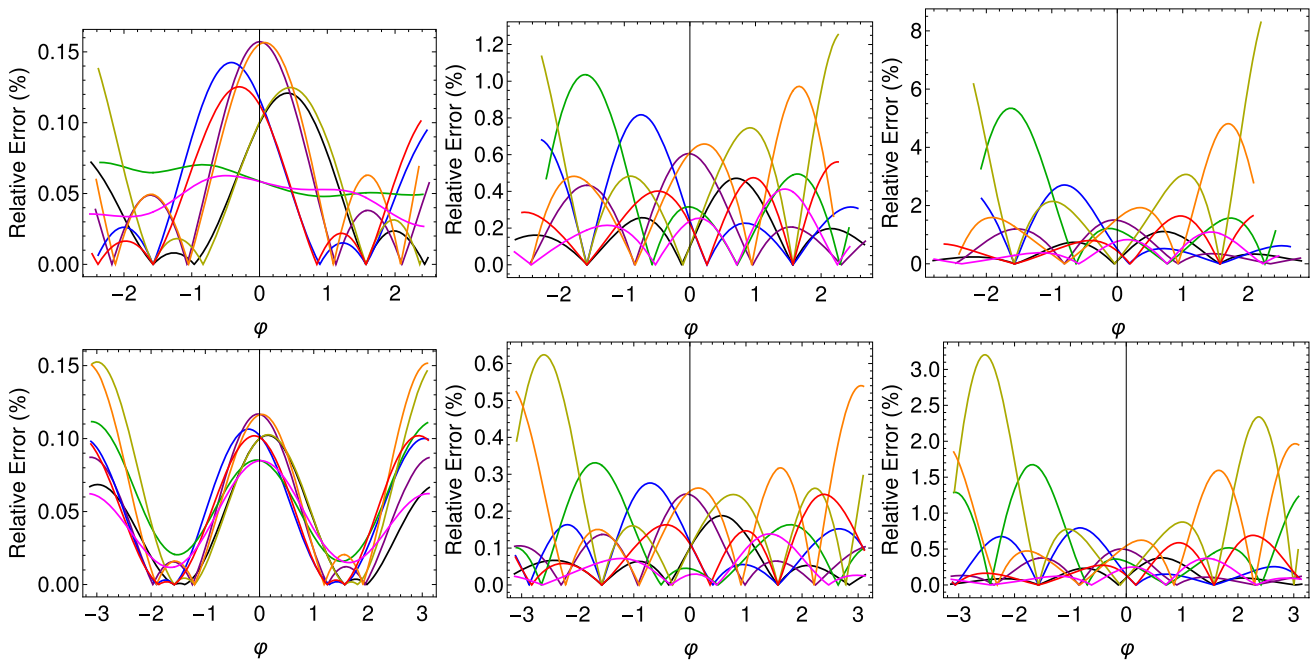

Fig. 4 Relative percentage error of redshift rapidity given by Eq. (66) for various values of orbital parameters p and e. The upper (lower) panels refer to $p = 100$ ($p = 1000$). Columns from left to right indicate $e = 0.1, 0.3$, and 0.5, respectively. $M = 1$, and $D = 1000p$. For various colors in each plot, see the bottom panel of Fig. 2

the relative error in frequency shift as follows

$$\frac{\delta z}{1+z} = \left| \frac{(1+z) - (1+z_{Schw})}{1+z} \right|, \tag{65}$$

where $1+z$ is the exact value calculated numerically using Eq. (42) and $1+z_{Schw}$ is obtained from the approximate expression Eq. (49). Similarly, the relative error in the redshift rapidity is defined as

$$\frac{\delta \dot{z}}{\dot{z}} = \left| \frac{\dot{z} - \dot{z}_{Schw}}{\dot{z}|_{\varphi=0}} \right|. \tag{66}$$

Here, $\dot{z}$ is the exact value of the redshift rapidity calculated numerically using Eq. (52), and $\dot{z}_{Schw}$ is defined by our approximate expression Eq. (63). The denominator is calculated at $\varphi = 0$ to avoid the divergence near $\varphi = \pi/2$ where $\dot{z}$ becomes zero (see Fig. 2). In Figs. 3 and 4, we have shown the relative percentage error against φ for various emitter orbits. As expected, the error is higher for higher e and lower p. As seen from the figures, the errors in frequency shift near the midline ($\varphi \approx \pm\pi/2$) are within 0.1% for $e = 0.1$, and 1% for $e = 0.3$, whereas it is relatively significant for $e = 0.5$ or above. Similarly, for redshift rapidity, the error remains within an acceptable range for eccentricity $e < 0.3$.

7 Discussion and final remarks

In this paper, we have presented two relations for the mass-to-distance ratio of the Schwarzschild black hole in terms of observable frequency shifts for three spacial points of the circular motion of orbiting massive particles: on the midline and close to the LOS. We further calculated the derivative of the frequency shift in the Schwarzschild background with respect to proper time in order to introduce the redshift rapidity. Then, we employed the redshift rapidity to express the Schwarzschild black hole mass and its distance from the Earth just in terms of observational quantities. In this formalism, the redshift rapidity is also a general relativistic invariant observable element, indicating the proper time evolution of the frequency shift in the Schwarzschild spacetime.

We have extracted concise and elegant analytic formulas that allow us to disentangle mass and distance to the black hole in the Schwarzschild background and compute these parameters separately, not the mass-to-distance ratio that we have estimated before in [24–27]. Our analytic formulas have been obtained on the midline and close to the LOS whereas the general relations could be employed in black hole parameter estimation studies.

We also computed the redshift and redshift rapidity for eccentric orbits of the emitter and calculated their relative error with respect to the numerical exact value of these quantities given by Eqs. (42) and (52), respectively. A simple analysis shows that the errors for these quantities at first order in e are within 1% for $e = 0.3$.

The next step in this research direction would be estimating the mass of supermassive Schwarzschild black holes hosted at the core of AGNs and their distance to the Earth with the help of the general relativistic formalism developed in the present paper. To do so, we need to perform a Bayesian statistical fit with the help of Eqs. (44) and (58) as well as precise measurements of the positions of the photon sources and their redshift and redshift rapidities. A task that we shall address in future works.

Acknowledgements We thank D. Villaraos and A. González-Juárez for fruitful discussions. All authors are grateful to CONACYT for support under Grant no. CF-MG-2558591; M.M. also acknowledges SNI and was supported by CONACYT through the postdoctoral Grants no. 31155 and no. 1242413. P.B. and A.H.-A. acknowledge financial support from the Science and Engineering Research Board, Government of India, File Number PDF/2022/000332. A.H.-A. and U.N. thank SNI and PRODEP-SEP and were supported by Grants VIEP-BUAP and CIC-UMSNH, respectively. U.N. also acknowledges support under Grant no. CF-140630.

Data Availability Statement This manuscript has no associated data. [Authors' comment: Data sharing not applicable to this article as no datasets were generated or analyzed during the current study.]

Code Availability Statement This manuscript has no associated code/software. [Author's comment: Code/Software sharing not applicable to this article as no code/software was generated or analyzed during the current study.]

Funded by SCOAP[3].

Appendix: ($\varphi + \delta$)-dependent light bending parameter and the angular distance δ as a function of the azimuthal angle φ

In a similar manner to [9], we obtain the light bending parameter for a general point of the circular orbit in the equatorial plane. However, unlike the previous work where the angular distance δ was neglected due to the large distances between the black holes and the Earth, we consider the contribution of this measurable parameter in our analysis. This is because even though the angular distance is very small, its variation

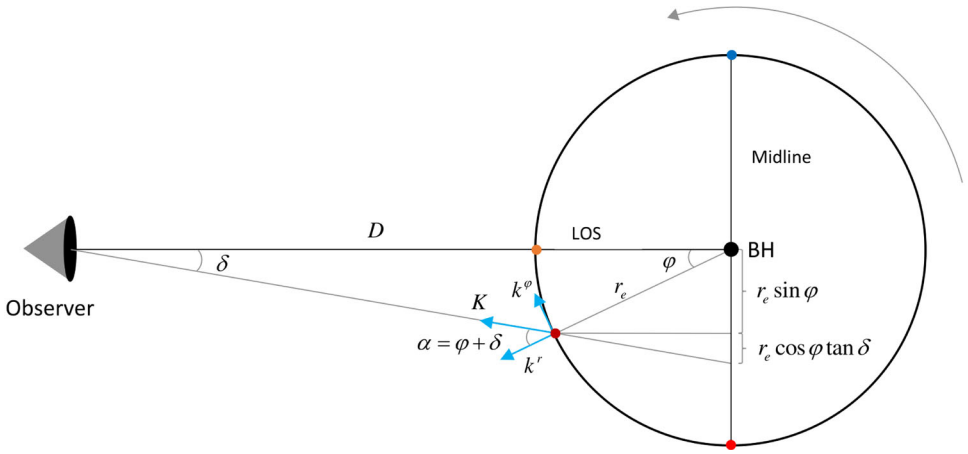

Fig. 5 The geometrical illustration of the bidimensional vector K, and the relation between the azimuthal angle φ and the angular distance δ

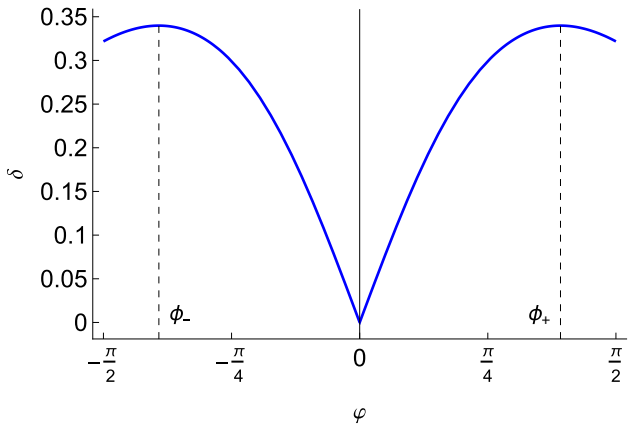

Fig. 6 The profile of the angular distance versus the azimuthal angle for $D = 3r_e$. The vertical dashed lines denote $\phi_\pm = \pm\arccos(1/3)$ where $d\delta/d\varphi$ vanishes

with respect to time, especially close to the LOS, is quite important. The other aim of this Appendix is to show the mathematical relation between the observable angular distance δ and the unobservable azimuthal angle φ if the emitter particle is far enough from the black hole.

In order to obtain the light bending parameter of photons coming from a general point of the circular orbit in the equatorial plane (see Fig. 5), we take into account the equation of motion of photons in the equatorial plane ($k^\theta = 0$) of the Schwarzschild spacetime (1)

$$g_{\mu\nu}k^\mu k^\nu = g_{tt}\left(k^t\right)^2 + g_{rr}\left(k^r\right)^2 + g_{\varphi\varphi}\left(k^\varphi\right)^2 = 0, \quad \text{(A.1)}$$

where k^t and k^φ can be found through the temporal Killing vector field $\xi^\mu = \delta^\mu_0$ and the rotational Killing vector field $\psi^\mu = \delta^\mu_3$ as follows

$$E_\gamma = -\xi_\mu k^\mu = -g_{tt}k^t, \quad \text{(A.2)}$$
$$L_\gamma = \psi_\mu k^\mu = g_{\varphi\varphi}k^\varphi, \quad \text{(A.3)}$$

which E_γ and L_γ are the energy and angular momentum of the photons, respectively.

By introducing (A.2) and (A.3) into (A.1), the equation of motion takes the following form

$$g_{rr}\left(k^r\right)^2 + \frac{E_\gamma^2}{g_{tt}} + \frac{L_\gamma^2}{g_{\varphi\varphi}} = 0, \quad \text{(A.4)}$$

that can be employed to express k^r in terms of the constants of motion and metric components as below

$$\left(k^r\right)^2 = -\frac{1}{g_{rr}}\left(\frac{E_\gamma^2}{g_{tt}} + \frac{L_\gamma^2}{g_{\varphi\varphi}}\right). \quad \text{(A.5)}$$

Now, by considering the non-vanishing angular distance $\delta \neq 0$, we geometrically introduce the auxiliary bidimensional vector K defined by the following decomposition (see Fig. 5 for more details)

$$k^r = K\cos\alpha, \quad \text{(A.6)}$$
$$r_e k^\varphi = K\sin\alpha, \quad \text{(A.7)}$$

with α the angle between the photon ray direction and its radial component at the emitter position and

$$K^2 = \left(k^r\right)^2 + r_e^2\left(k^\varphi\right)^2. \quad \text{(A.8)}$$

Hence, by substituting Eqs. (A.3) and (A.5) into (A.8), one can find K^2 versus the constants of motion and metric components as follows

$$K^2 = -\frac{1}{g_{rr}}\left(\frac{E_\gamma^2}{g_{tt}} + \frac{L_\gamma^2}{g_{\varphi\varphi}}\right) + r_e^2\frac{L_\gamma^2}{g_{\varphi\varphi}^2}. \quad \text{(A.9)}$$

On the other hand, by introducing Eq. (A.6) into (A.5), we can find a similar relation for K^2 as

$$K^2 = -\frac{1}{g_{rr}\cos^2\alpha}\left(\frac{E_\gamma^2}{g_{tt}} + \frac{L_\gamma^2}{g_{\varphi\varphi}}\right). \quad \text{(A.10)}$$

Equating previous relations gives an equation for the α-dependent light bending parameter b_γ as below

$$\left(g_{tt}b_\gamma^2 + g_{\varphi\varphi}\right)g_{\varphi\varphi}\tan^2\alpha + r_e^2 g_{rr}g_{tt}b_\gamma^2 = 0, \quad \text{(A.11)}$$

that leads to the following solution for b_γ

$$b_\gamma = \frac{-g_{\varphi\varphi}\sin\alpha}{\sqrt{-g_{tt}}\sqrt{g_{\varphi\varphi}\sin^2\alpha + r_e^2 g_{rr}\cos^2\alpha}}, \tag{A.12}$$

which is the light bending parameter for an arbitrary point of the circular orbit on the equatorial plane.

On the other hand, if we assume the emitter is far enough from the black hole and consider the geometrical configuration illustrated in Fig. 5 we can write $\alpha \approx \varphi + \delta$, where, as mentioned earlier, δ is the is the observable angular distance and φ is the unobservable azimuthal angle.

In this case, we can obtain a relation between δ and φ. This is necessary to express φ in terms of the observable quantity δ in order to obtain M and D just in terms of observational elements, hence being able to break the degeneracy of the M/D ratio.

By taking into account the right triangle in Fig. 5, one can immediately identify the following relation between the set $\{D, r_e; \varphi, \delta\}$

$$D\tan\delta = r_e\left(\sin\varphi + \cos\varphi\tan\delta\right), \tag{A.13}$$

where only δ is observable and the rest of the parameters are unknown in the case of black holes since we cannot identify the black hole position by observations. After doing some straightforward simplifications, this relation reduces to

$$D\sin\delta = r_e\sin\left(\varphi + \delta\right), \tag{A.14}$$

in which for the far away detectors where $D \gg r_e$ and $\delta \to 0$, we have

$$r_e \approx D\delta_m\left(1 + \frac{\delta_m^2}{3}\right), \quad \text{for } \varphi = \pm\frac{\pi}{2}, \tag{A.15}$$

$$r_e \approx \frac{D\delta_s}{\varphi_s}, \quad \text{for } \varphi \to 0, \tag{A.16}$$

for the midline $\varphi = \pm\pi/2$ and close to the LOS $\varphi \to 0$, respectively.

Now, we solve the relation (A.14) in order to express δ in terms of the rest of the parameters. This equality has four solutions, and we choose the physical one as below

$$\delta = \arccos\left(\frac{D - r_e\cos\varphi}{\sqrt{D^2 + r_e^2 - 2Dr_e\cos\varphi}}\right), \tag{A.17}$$

since as φ decreases/increases, δ should also decrease/increase in the same direction (see Fig. 5).

Figure 6 illustrates the behavior of δ versus φ. As one can see from this figure, if we solve the azimuthal angle φ in terms of δ, we shall have four expressions as follows

$$\varphi = \begin{cases} \pm\delta \mp \arcsin\left(\frac{D\sin\delta}{r_e}\right), & \phi_- \le \varphi \le \phi_+ \\ \pm\pi \mp \delta \mp \arcsin\left(\frac{D\sin\delta}{r_e}\right), & \begin{cases} -\frac{\pi}{2} \le \varphi \le \phi_- \\ \phi_+ \le \varphi \le \frac{\pi}{2} \end{cases} \end{cases} \tag{A.18}$$

to cover the whole semicircular path from $\varphi = -\pi/2$ to $\varphi = \pi/2$. In these relations, ϕ_+ (ϕ_-) denotes a special point where $d\delta/d\varphi$ vanishes for $\varphi > 0$ ($\varphi < 0$), as indicated in Fig. 6.

References

1. B.P. Abbott et al. (LIGO Scientific and Virgo Collaborations), Observation of gravitational waves from a binary black hole merger. Phys. Rev. Lett. **116**, 061102 (2016)
2. K. Akiyama et al. (Event Horizon Telescope Collaboration), First M87 event horizon telescope results. IV. Imaging the central supermassive black hole. Astrophys. J. Lett. **875**, L4 (2019)
3. K. Akiyama et al. (Event Horizon Telescope Collaboration), First Sagittarius A* event horizon telescope results. VI. Testing the black hole metric. Astrophys. J. Lett **930**, L17 (2022)
4. A.M. Ghez, S. Salim, N.N. Weinberg, J.R. Lu, T. Do, J.K. Dunn, K. Matthews, M.R. Morris, S. Yelda, E.E. Becklin, T. Kremenek, M. Milosavljevic, J. Naiman, Measuring distance and properties of the Milky Way's central supermassive black hole with stellar orbits. Astrophys. J. **689**, 1044 (2008)
5. M.R. Morris, L. Meyer, A.M. Ghez, Galactic center research: manifestations of the central black hole. Res. Astron. Astrophys. **12**, 995 (2012)
6. A. Eckart, R. Genzel, Observations of stellar proper motions near the galactic centre. Nature **383**, 415 (1996)
7. S. Gillessen, F. Eisenhauer, S. Trippe, T. Alexander, R. Genzel, F. Martins, T. Ott, Monitoring stellar orbits around the massive black hole in the galactic center. Astrophys. J. **692**, 1075 (2009)
8. A. Herrera-Aguilar, U. Nucamendi, Kerr black hole parameters in terms of the redshift/blueshift of photons emitted by geodesic particles. Phys. Rev. D **92**, 045024 (2015)
9. P. Banerjee, A. Herrera-Aguilar, M. Momennia, U. Nucamendi, Mass and spin of Kerr black holes in terms of observational quantities: the dragging effect on the redshift. Phys. Rev. D **105**, 124037 (2022)
10. M. Momennia, A. Herrera-Aguilar, U. Nucamendi, Kerr black hole in de Sitter spacetime and observational redshift: toward a new method to measure the Hubble constant. Phys. Rev. D **107**, 104041 (2023)
11. J.R. Herrnstein, J.M. Moran, L.J. Greenhill, A.S. Trotter, The geometry of and mass accretion rate through the maser accretion disk in NGC 4258. Astrophys. J. **629**, 719 (2005)
12. A.L. Argon, L.J. Greenhill, M.J. Reid, J.M. Moran, E.M.L. Humphrey, Toward a new geometric distance to the active Galaxy NGC 4258. I. VLBI monitoring of water maser emission. Astrophys. J **659**, 1040 (2007)
13. E.M.L. Humphreys, M.J. Reid, J.M. Moran, L.J. Greenhill, A.L. Argon, Toward a new geometric distance to the active galaxy NGC 4258. III. Final results and the Hubble constant. Astrophys. J **775**, 13 (2013)
14. G.V. Kraniotis, Gravitational redshift/blueshift of light emitted by geodesic test particles, frame-dragging and pericentre-shift effects, in the Kerr–Newman–de Sitter and Kerr–Newman black hole geometries. Eur. Phys. J. C **81**, 147 (2021)
15. D. Ujjal, Motion and collision of particles near Plebanski–Demianski black hole: shadow and gravitational lensing. Chin. J. Phys. **70**, 213 (2021)
16. M. Sharif, S. Iftikhar, Dynamics of particles near black hole with higher dimensions. Eur. Phys. J. C **76**, 404 (2016)
17. R. Becerril, S. Valdez-Alvarado, U. Nucamendi, P. Sheoran, J.M. Davila, Mass parameter and the bounds on redshifts and blueshifts

of photons emitted from geodesic particle orbiting in the vicinity of regular black holes. Phys. Rev. D **103**, 084054 (2021)
18. P. Sheoran, A. Herrera-Aguilar, U. Nucamendi, Mass and spin of a Kerr black hole in modified gravity and a test of the Kerr black hole hypothesis. Phys. Rev. D **97**, 124049 (2018)
19. L.A. Lopez, J.C. Olvera, Frequency shifts of photons emitted from geodesics of nonlinear electromagnetic black holes. Eur. Phys. J. Plus **136**, 64 (2021)
20. L.A. Lopez, N. Breton, Redshift of light emitted by particles orbiting a black hole immersed in a strong magnetic field. Astrophys. Space Sci. **366**, 55 (2021)
21. R. Becerril, S. Valdez-Alvarado, U. Nucamendi, Obtaining mass parameters of compact objects from red-blue shifts emitted by geodesic particles around them. Phys. Rev. D **94**, 124024 (2016)
22. Q.M. Fu, X. Zhang, Probing a polymerized black hole with the frequency shifts of photons. Phys. Rev. D **107**, 064019 (2023)
23. D.A. Martinez-Valera, M. Momennia, A. Herrera-Aguilar, Observational redshift from general spherically symmetric black holes. Eur. Phys. J. C **84**, 288 (2024)
24. U. Nucamendi, A. Herrera-Aguilar, R. Lizardo-Castro, O. Lopez-Cruz, Toward the gravitational redshift detection in NGC 4258 and the estimation of its black hole mass-to-distance ratio. Astrophys. J. Lett. **917**, L14 (2021)
25. A. Villalobos-Ramirez, O. Gallardo-Rivera, A. Herrera-Aguilar, U. Nucamendi, A general relativistic estimation of the black hole mass-to-distance ratio at the core of TXS 2226–184. Astron. Astrophys. **662**, L9 (2022)
26. D. Villaraos, A. Herrera-Aguilar, U. Nucamendi, G. Gonzalez-Juarez, R. Lizardo-Castro, A general relativistic mass-to-distance ratio for a set of megamaser AGN black holes. MNRAS **517**, 4213 (2022)
27. A. Gonzalez-Juarez, M. Momennia, A. Villalobos-Ramirez, A. Herrera-Aguilar, The mass-to-distance ratio for a set of megamaser AGN black holes by employing a general relativistic method. arXiv:2211.06486
28. G. Morales-Herrera, P. Ortega-Ruiz, M. Momennia, A. Herrera-Aguilar, Mass, charge, and distance to Reissner–Nordström black hole in terms of directly measurable quantities. Eur. Phys. J. C **84**, 525 (2024). arXiv:2401.07112
29. J.A. Braatz, M.J. Reid, E.M.L. Humphreys, C. Henkel, J.J. Condon, K.Y. LO, The megamaser cosmology project. II. The angular-diameter distance to UGC 3789. Astrophys. J **718**, 657 (2010)
30. C.Y. Kuo, J.A. Braatz, M.J. Reid, K.Y. Lo, J.J. Condon, C.M.V. Impellizzeri, C. Henkel, The megamaser cosmology project. V. An angular-diameter distance to NGC 6264 at 140 Mpc. Astrophys. J. **767**, 155 (2013)
31. F. Gao, J.A. Braatz, M.J. Reid, K.Y. Lo, J.J. Condon, C. Henkel, C.Y. Kuo, C.M.V. Impellizzeri, D.W. Pesce, W. Zhao, The megamaser cosmology project. VIII. A geometric distance to NGC 5765b. Astrophys. J. **817**, 128 (2016)
32. M.J. Reid, D.W. Pesce, A.G. Riess, An improved distance to NGC 4258 and its implications for the Hubble constant. Astrophys. J. Lett. **886**, L27 (2019)
33. D.W. Pesce, J.A. Braatz, M.J. Reid, J.J. Condon, F. Gao, C. Henkel, C.Y. Kuo, K.Y. Lo, W. Zhao, The Megamaser Cosmology Project. XI. A geometric distance to CGCG 074-064. Astrophys. J. **890**, 118 (2020)